ACS APPLIED MATERIALS & INTERFACES

Research Article

www.acsami.org

Bacterially Antiadhesive, Optically Transparent Surfaces Inspired from Rice Leaves

Jun Kyun Oh,[†] Xiaoxu Lu,[‡] Younjin Min,[‡] Luis Cisneros-Zevallos,[§] and Mustafa Akbulut*[,†,∥]

[†]Department of Materials Science and Engineering, Texas A&M University, College Station, Texas 77843, United States

[‡]Department of Polymer Engineering, The University of Akron, Akron, Ohio 44325, United States

[§]Department of Horticultural Sciences, Texas A&M University, College Station, Texas 77843, United States

[∥]Artie McFerrin Department of Chemical Engineering, Texas A&M University, College Station, Texas 77843, United States

Supporting Information

ABSTRACT: Because of the growing prevalence of antimicrobial resistance strains, there is an increasing need to develop material surfaces that prevent bacterial attachment and contamination in the absence of antibiotic agents. Herein, we present bacterial antiadhesive materials inspired from rice leaves. "Rice leaf-like surfaces" (RLLS) were fabricated by a templateless, self-masking reactive-ion etching approach. Bacterial attachment on RLLS was characterized under both static and dynamic conditions using Gram-negative *Escherichia coli* O157:H7 and Gram-positive *Staphylococcus aureus*. RLLS surfaces showed exceptional bacterial antiadhesion properties with a >99.9% adhesion inhibition efficiency. Furthermore, the optical properties of RLLS were investigated using UV−vis−NIR spectrophotometry. In contrast to most other bacterial antiadhesive surfaces, RLLS demonstrated optical-grade transparency (i.e., ≥92% transmission). We anticipate that the combination of bacterial antiadhesion efficiency, optical grade transparency, and the convenient single-step method of preparation makes RLLS a very attractive candidate for the surfaces of biosensors; endoscopes; and microfluidic, bio-optical, lab-on-a-chip, and touchscreen devices.

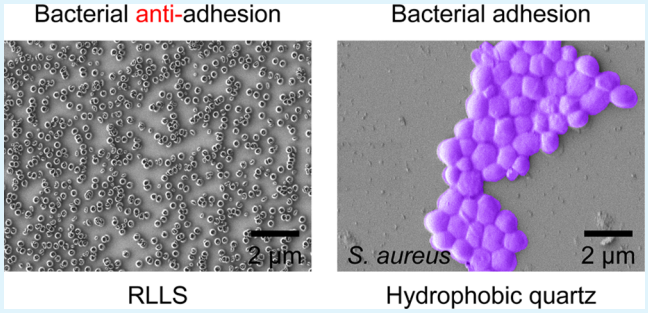

KEYWORDS: *bioinspiration, bacterial fouling, optical transparency, biosensors, endoscopes*

1. INTRODUCTION

Bacterial fouling is responsible not only for the functional deterioration of numerous surfaces and devices but also for the transmission of infection and disease through such surfaces and devices.[1] Bacterial adhesion to a surface, which is the first step in bacterial fouling, is governed by the interplay among the physicochemical, interfacial, and geometrical characteristics of the surface and bacteria.[2] Hence, various surface-modification approaches have been applied and considered to manipulate the interactions between bacteria and surfaces and to prevent bacterial attachment to surfaces.[3−5] To this end, in particular, surfaces based on nature-inspired approaches have shown promising potential in the reduction and inhibition of bacterial adhesion.[6,7] In the light of increasing global concerns about antimicrobial resistance,[8] such surfaces are increasingly needed to provide alternative or complementary solutions to antimicrobial surfaces.

One of the key challenges for nature-inspired bacterial antiadhesive surfaces is the integration of transparency and the bacterial antiadhesion within a single surface. This is primarily because surface texture and roughness including the ones inspired from biological materials often lead to light scattering as predicted by analytic scattering models and rigorous electromagnetic theories.[9,10] The transparency is generally inversely correlated with the scattering of light.[11] With the increasing number of emerging biomedical applications and optical devices requiring high levels of transparency, as well as operations in bacterial media,[12,13] the need for overcoming this challenge has intensified.

Plant tissues display an unique and rich variety of optical properties governed by their ultrastructure.[14] When light travels across different tissue layers, its characteristics are modified. Depending on the photosynthetic or photomorphogenic needs, a tissue layer can be responsible for light propagation, light trapping, light gradients, focusing and lens effects, and wavelength-specific surface reflection.[15] For instance, to achieve the efficient use of light energy, upper layers of most leaves (i.e., cuticle and epidermis) are often designed to allow an efficient passage of light.[16] On the other hand, the mesophyll, which is packed with chloroplasts, is responsible for the scattering and absorption of light.[17] One can hypothesize that it is possible to

Received: June 12, 2015
Accepted: August 3, 2015
Published: August 3, 2015

DOI: 10.1021/acsami.5b05198
ACS Appl. Mater. Interfaces 2015, 7, 19274−19281

use the guiding principles behind plant tissues to design new optical materials through bioinspiration.

Herein, we report a rice leaf-inspired approach to produce novel surfaces with optical transparency and repellency against bacterial suspensions. The rice leaf was especially selected for bioinspiration due to its unique hollow nanodisc texture, which reduces "the total roughness volume" compared to solid pillar-type bioinspirations. The biomimetic "rice leaf-like surfaces" (RLLS) showed strong water and bacterial suspension repellency with static contact angles of 155.7° ± 1.2° and 150.6° ± 1.0°, respectively. In addition, RLLS displayed excellent bacterial antiadhesion properties with an adhesion inhibition efficiency of >99.9% for both pathogenic Gram-negative *Escherichia coli* O157:H7 and Gram-positive *Staphylococcus aureus* in comparison to pristine quartz surfaces (negative control). In this study, these two microorganisms were selected for two reasons: first, pathogenic bacterial strains tend to adhere to surfaces more strongly than nonpathogenic ones;[18] and second, according to the United States Centers for Disease Control and Prevention (CDC), the most common pathogens that cause hospital-acquired infections are *E. coli*, *S. aureus*, and *Pseudomonas aeruginosa*. Furthermore, RLLS demonstrated optical-grade transparency (i.e., ≥92% transmission) due to the relatively small roughness volume achieved through hollow nanodisc morphology.

2. EXPERIMENTAL SECTION

2.1. Leaf Materials from Rice Plant. Fully developed rice leaf (*Oryza sativa* L. ssp. *japonica* cv. Calmati-202) was obtained from the Division of Agriculture and Natural Resources at University of California, Davis, CA, U.S.A. The received rice leaves were kept in a water bath before use. Fresh leaves were cut into 5 mm × 5 mm flat areas and immediately used afterward to prevent drying.

2.2. Bioinspired Surface Preparation. Quartz (SiO_2) slides (Ted Pella, Inc., Redding, CA, U.S.A.) cut into 1 cm × 1 cm × 1 mm were first rinsed with water purified by a Milli-Q Advantage system A10 (EMD Millipore Corp., Billerica, MA, U.S.A.), yielding Milli-Q water with resistivity of 18.2 MΩ·cm, and left to dry at room temperature (23 °C). Subsequently, oxygen plasma treatment by CS-1701 reactive-ion etcher (RIE; Nordson MARCH, Concord, CA, U.S.A.) was applied to remove organic adsorbates on the surfaces: these slides were used as hydrophilic quartz controls. "Rice leaf-like surfaces" (RLLS) were fabricated by self-masking reactive-ion etching (SM-RIE) of quartz surfaces for which the operational parameters were critical in manipulating surface morphology. The following conditions gave rise to RLLS: flow rates of tetrafluoromethane (CF_4) at 22.5 sccm and oxygen (O_2) at 2.5 sccm, pressure of 80 mTorr, radio frequency (RF) power of 200 W, and etching time of 20 min.

To enable superhydrophobicity, the etched quartz surfaces with rice leaf-like surface texture were functionalized with trimethylsilyl chloride (TMCS; Sigma-Aldrich Co., St. Louis, MO, U.S.A.) by placing these in 6% TMCS in hexane (Avantor Performance Materials, Inc., Center Valley, PA, U.S.A.). The silanation reaction was allowed to take place for 24 h. Afterward, surfaces were rinsed with hexane and dried under a stream of nitrogen gas (N_2; Brazos Valley Welding Supply, Inc., Bryan, TX, U.S.A.) before use. The same functionalization procedure was also used for the smooth (unetched) quartz surfaces to create hydrophobic quartz controls.

2.3. Physical and Chemical Characterization of Surfaces. Surface morphology of the samples was characterized using scanning electron microscope (SEM; JSM-7500F, JEOL, Tokyo, Japan). In SEM experiments, the surfaces were coated with 8 nm of platinum/palladium (Pt/Pd) to reduce charging effects.

The surface roughness was quantified by atomic force microscopy (AFM; Dimension Icon, Bruker, Santa Barbara, CA, U.S.A.). Amplitude and height images were obtained in the tapping mode. The silicon tip cantilever with nominal spring constant of 0.4 N/m, nominal tip radius of 2 nm, and the nominal resonant frequency of 70 kHz were used.

The TMCS functionalized silica-based materials (i.e., quartz and RLLS) were characterized using attenuated total reflectance-Fourier transform infrared (ATR-FTIR) spectroscopy. ATR-FTIR spectra were recorded on an IRPrestige-21 (Shimadzu Corp., Kyoto, Japan) system and analyzed using IRsolution (Shimadzu Corp., Kyoto, Japan) software version 1.40.

X-ray photoelectron spectroscopy (XPS) measurements of TMCS coverage on silica surfaces were characterized using PHI VersaProbe II Scanning XPS Microprobe (Physical Electronics, Chanhassen, MN, U.S.A.). The measurements were carried out using an Al Kα radiation source (1486.6 eV) operating at 25 W and under high-vacuum conditions at a pressure of 10^{-7} Pa.

To determine the wetting characteristics of surfaces, static and dynamic contact angles of water and bacterial suspension were measured.[19] The contact angles were analyzed by contact angle plug-in for ImageJ (National Institutes of Health (NIH), Bethesda, MD, U.S.A.) software. The contact angle values reported on each surface were obtained by averaging six measurements at room temperature (23 °C).

2.4. Growth and Maintenance of Microorganisms. *Escherichia coli* O157:H7 and *Staphylococcus aureus* were obtained from the Food Microbiology Laboratory Culture Collection in the Department of Animal Science at Texas A&M University, College Station, TX, U.S.A. Working cultures of *E. coli* O157:H7 and *S. aureus* were grown in tryptic soy broth (TSB; Becton, Dickinson and Co., Sparks, MD, U.S.A.) with 24 h incubation aerobically at 37 °C. A loopful of bacterial culture in TSB was transferred twice to fresh TSB every 24 h and reincubated at 37 °C, resulting in bacterial suspensions to a final concentration of 8.7−9.1 log CFU/mL.

2.5. Bacterial Adhesion Assay under Static Conditions. Rice leaves cut into 5 mm × 5 mm were immersed in 9.0 mL of bacterial suspensions (8.7−9.1 log CFU/mL) and incubated for 4 h at room temperature (23 °C). The treated rice leaves were then gently removed from the bacterial suspensions to count attached bacteria on surfaces. When removing the samples, we made sure that samples were drawn in a single vertical motion from the bacterial suspension and held vertically for 3 min to allow remaining droplets to slide away so that drying effects were not superimposed on the results of adhesion. All inoculation experiments were replicated four times. The same experimental procedure was used for pristine quartz, hydrophobic quartz, and RLLS.

SEM was employed to quantify the attachment of *E. coli* O157:H7 and *S. aureus* on various surfaces. After acrolein (Sigma-Aldrich Co., St. Louis, MO, U.S.A.) inactivation, 10 nm of gold (Au) coating was applied to sample surfaces to ensure electrical conductivity required by SEM technique. For quantitative analysis, 100 μm × 100 μm of SEM images from at least nine different areas were analyzed to count the number of attached bacteria. Experiments were repeated three times for each sample.

2.6. Bacterial Adhesion Assay under Dynamic Conditions. Flow experiments were carried out using a custom flow chamber with 1 cm × 1 cm window made out of the material of interest. Bacterial adhesion behavior on RLLS window was compared with pristine quartz window (uncoated) and hydrophobic quartz window (methylated) by replacing the chamber window in each experiment. For all surfaces, the flow rate of bacterial suspension inside the chamber was controlled to be 2.5 μL/s.

Images of flowing bacteria were visualized using differential interference contrast (DIC) microscopy (Stallion Digital Imaging Workstation; Carl Zeiss, Jena, Germany) at a frame rate of 0.5 fps. Movies created by stacking images obtained at various time points were analyzed manually with ImageJ software to count attached bacteria on surfaces.

2.7. Screening of Antimicrobial Activity. To determine if antimicrobial activity or bacterial antiadhesion is responsible for the observed trends, *E. coli* O157:H7 and *S. aureus* strains were grown in the presence of TMCS-functionalized RLLS and in the presence of 1% (v/v) bleach solution for 4 h at room temperature (23 °C). Bacteria in

DOI: 10.1021/acsami.5b05198
ACS Appl. Mater. Interfaces 2015, 7, 19274−19281

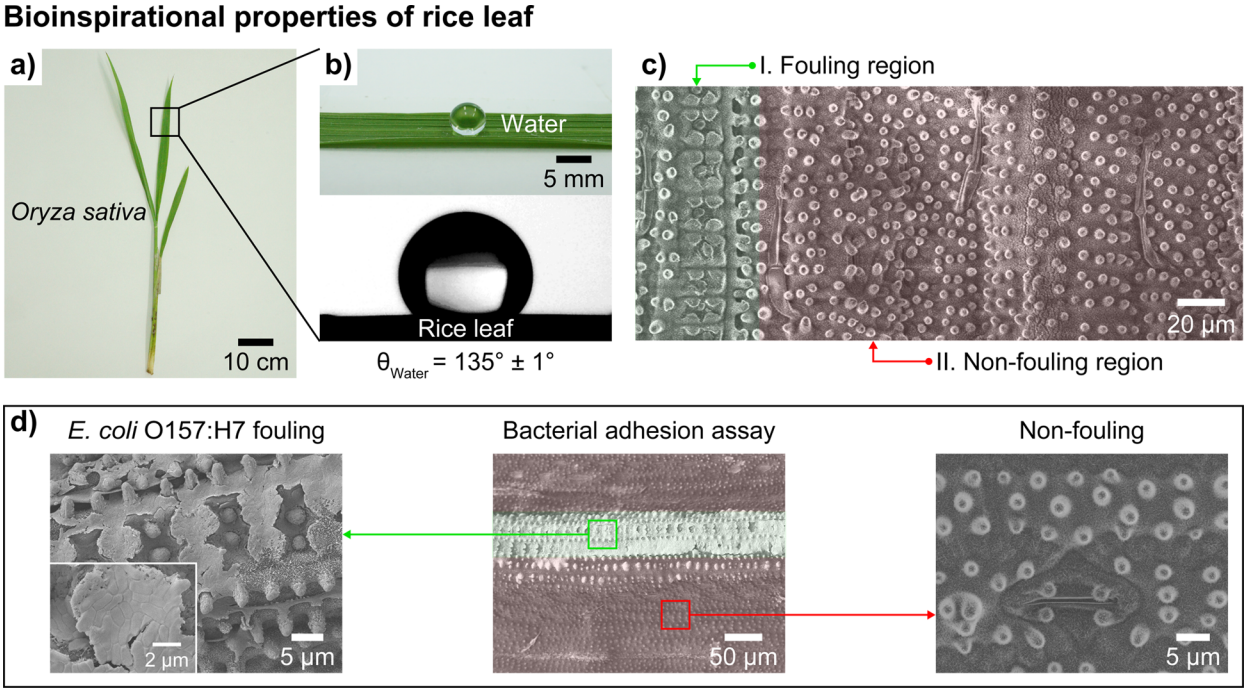

Figure 1. (a) Photograph of *Oryza sativa* rice leaf, (b) wetting characteristics of water on rice leaf, (c) SEM micrograph showing the texture (ultrastructure) of rice leaf, and (d) bacterial attachment behavior on rice leaf.

the absence of any treatment were used as negative controls. To count the number of bacteria remaining, pour plate method was used by taking 1.0 mL of bacterial suspension from each dilution to make serial dilutions. The results are reported as colony-forming units per milliliter (CFU/mL) and replicated three times.

2.8. Optical Transparency. Transparency of material was studied by measuring transmittance via UV−vis−NIR spectrophotometry (U-4100; Hitachi, Tokyo, Japan). Transmission spectra were recorded at a wavelength range of 400−800 nm.

2.9. Pressure and Chemical Stability Tests. Autoclaving is one of the most effective and common methods for sterilization. To confirm mechanical stability of RLLS upon autoclaving, RLLS was placed in an autoclave (Amsco Lab 250; Steris Corp., Mentor, OH, U.S.A.) chamber at 121 °C for 20 min under 20 psi pressure conditions.

Chemical stability of RLLS immersed in 10% hydrogen peroxide (H_2O_2, 30% solution; Avantor Performance Materials, Inc., Center Valley, PA, U.S.A.) solution was monitored as a function of time. To confirm if any of surface groups are detaching from RLLS with time, aliquots from the solution containing immersed RLLS were collected and analyzed using ATR-FTIR spectroscopy at 4 h, 3 days, 1 week, 2 weeks, and 3 weeks.

2.10. Statistical Analysis. Statistical analysis was performed by using the statistical package for Microsoft Office Excel (Microsoft Corp., Redmond, WA, U.S.A.) software. Microbiological data from microscope images were log-transformed prior to statistical analysis. One-way and two-way analysis of variance (ANOVA) with Tukey's post hoc test was used to determine statistical significance of differences between microbiological data from surface types and types of bacteria at a p-value of <0.05.

3. RESULTS AND DISCUSSION

3.1. Interfacial and Bacterial Adhesion Characteristics of Rice Leaf. Plant surfaces, highly sophisticated structures, are responsible for multiple functions such as the reduction of water loss, the control of surface wetting, the recognition of pathogens and insects, the inhibition of contaminant adhesion, the maintenance of physiological integrity, and the reduction of surface temperature. These functions are strongly dependent on surface chemistry and structure.[20] As such, our initial focus was on the interfacial characteristics of rice leaves (*Oryza sativa*), which resulted in a water contact angle of 135.1° ± 1.4° on them under static conditions, indicating their highly hydrophobic nature (Figure 1a, b). The morphology responsible for such a wetting behavior involved multiple length scales: (i) submillimeter-scale groove array with an average width of 155.4 ± 14.2 μm and depth of 19.6 ± 1.7 μm, (ii) highly ordered, micron-scale, and clover-shaped features located on the apex of grooves with a radius of 6.3 ± 0.5 μm, and (iii) hollow microdiscs located at the bottom and sides of grooves with an outer diameter of 3.4 ± 0.5 μm, inner diameter of 1.5 ± 0.4 μm, and height of 3.4 ± 0.6 μm (Figure 1c and Figure S1). Previous studies on rice leaves reported that the microdiscs and microclovers are responsible for their super-hydrophobicity while the groove arrays provide an energy barrier to travel in orthogonal directions and contribute to the anisotropic sliding phenomenon.[21]

It is known that surface roughness and texture can greatly influence bacterial adhesion.[22] Hence, after characterizing the surface structure of rice leaves, we focused on their bacterial adhesion behavior. As shown in Figure 1d, there were two distinct behaviors: while there was significant bacterial (*E. coli* O157:H7) adhesion on the regions where microclovers are located, i.e., the apex of grooves, there was no detectable bacterial adhesion on the regions where microdiscs are located, i.e., the bottom and sides of grooves. This trend can be attributed to the morphological characteristics of bacterial antiadhesion regions: micropillar-type structures including microdiscs are known to often cause the transition from the Wenzel state to the Cassie−Baxter state, where the formation of air pockets can prevent bacterial attachment.[23] In addition, due to their hollow nature, the total volume of air pockets on hollow microdiscs can be enhanced in comparison to the Cassie−Baxter state of solid microdiscs and micropillars, thereby further inhibiting bacterial access to the surface. In

DOI: 10.1021/acsami.5b05198
ACS Appl. Mater. Interfaces 2015, 7, 19274−19281

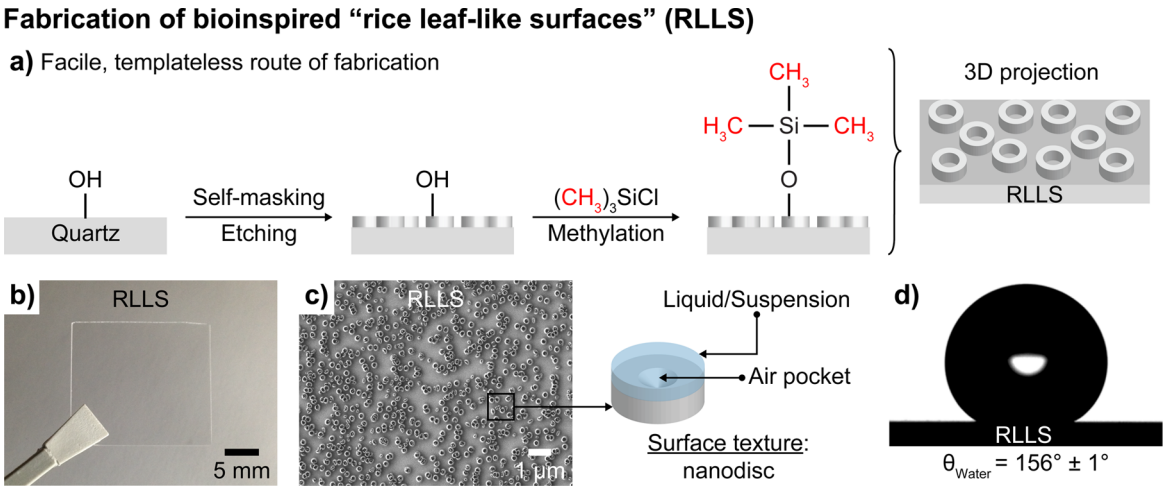

Figure 2. (a) Fabrication process of bioinspired "rice leaf-like surfaces" (RLLS), (b) photograph of RLLS, (c) SEM micrograph of RLLS surface, and (d) wetting characteristics of water on RLLS. Statistical analysis of SEM and AFM micrographs revealed that inner diameter of nanodiscs was 163.0 ± 10.5 nm, outer diameter was 198.2 ± 9.3 nm, height was 436.7 ± 12.6 nm, average spacing between nanodiscs was 214.6 ± 153.4 nm, and ratio of the total rim area to total projection area was ~0.06.

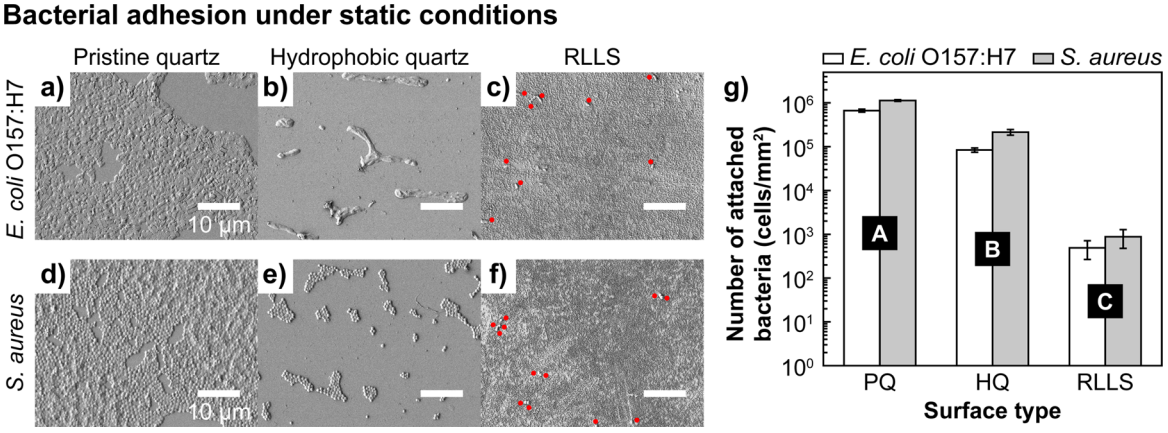

Figure 3. SEM micrographs of bacterial attachment on pristine quartz (PQ), hydrophobic quartz (HQ), and RLLS surfaces for (a–c) *E. coli* O157:H7 and (d–f) *S. aureus* (bacteria on RLLS surfaces were highlighted with red). (g) The bacterial attachment density as a function of surface type. Different letters (i.e., A, B, and C) indicate statistically significant differences ($p < 0.05$).

addition to the surface structure, there may be additional factors responsible for the observed trend such as surface chemistry of microdiscs (see Supporting Information for further discussion).

3.2. Fabrication of RLLS. Bioinspired surfaces are typically fabricated via bottom-up approaches such as layer-by-layer assembly and nanoparticle deposition, direct replicating method using polymers (e.g., polydimethylsiloxane, poly(vinyl alcohol), and polyurethane), and top-down approaches such as soft lithography.[24] The main limitation of bottom-up approaches is the challenges associated with their scale-up and mass production.[25] Direct replicating method allows only the exact replication of surface texture. When a modification in the texture size or dimension of the fabricated surface is needed, this approach becomes unfeasible. Furthermore, direct replication often relies on soft, low adhesion energy polymers to enable their peeling off from the original pattern.[26] However, such soft polymers tend to suffer from the lack of mechanical and scratch resistance.[27] Top-down photolithography, the most common method to fabricate nature-inspired surfaces, requires multiple steps, i.e., exposure, development, deposition, and lift-off.[28]

Here, we describe a self-masking reactive-ion etching (SM-RIE) approach that overcomes the above-mentioned limitations (Figure 2a). The principles driving the formation of hollow nanodiscs were that (i) due to the preferential vertical transport of ions, RIE gives rise to anisotropic etch profiles;[29] (ii) due to its crystal structure, the etching rates show variations in different crystal planes of quartz;[30] and (iii) RIE using CF_4 often leads to the polymerization of fluorocarbons (C_xF_y),[31] which can form nano/microdroplets on quartz and act as masks for directing etching.[32,33] SM-RIE allowed a strong control over topographical and structural characteristics of the surfaces by adjusting etching time, CF_4/O_2 flow rates, pressure, and radio frequency (RF) power (Figure S2). At relatively low CF_4/O_2 flow rates and low RF power, it was possible to produce hollow nanodiscs that mimicked rice leaf in a single-step process (Figure 2b, c).

3.3. Wetting Characteristics of RLLS. Hydrophilic materials tend to aggregate on hydrophilic surfaces.[34] While bacteria can adhere on both hydrophobic and hydrophilic surfaces, bacterial attachment tends to occur significantly more on hydrophilic surfaces due to their hydrophilic nature.[35] Therefore, it is necessary to investigate the wetting character-

DOI: 10.1021/acsami.5b05198
ACS Appl. Mater. Interfaces 2015, 7, 19274–19281

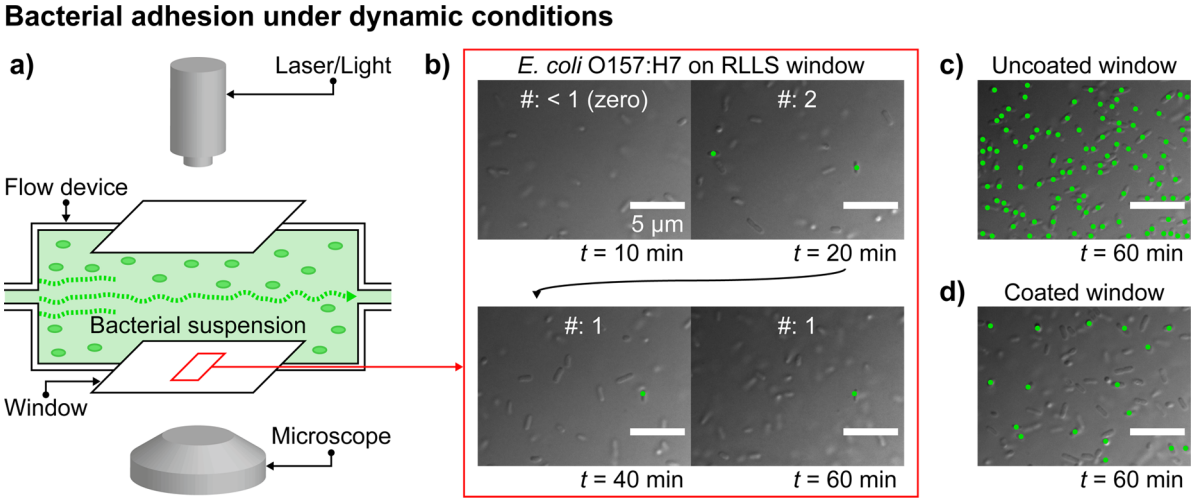

Figure 4. (a) Schematic illustration of the experimental setup used in studying bacterial adhesion under dynamic conditions. (b) Time-resolved micrographs of bacterial attachment on RLLS window obtained via differential interference contrast (DIC) microscopy. The fully adhered bacteria are highlighted with green. Comparison of bacterial attachment on RLLS with (c) uncoated window and (d) coated window (methylated) at a dynamic bacterial exposure time of 60 min. See Supporting Information for movie files.

istics of the developed surfaces to gain insight into their bacterial adhesion behaviors. The static water contact angle measurements revealed that, while the pristine quartz was hydrophilic (θ < 10.0°), methylated quartz (θ = 95.9° ± 1.1°) and RLLS (θ = 155.7° ± 1.2°) were hydrophobic and superhydrophobic, respectively (Figure 2d). The superrepellency of surfaces was also valid for concentrated *E. coli* O157:H7 suspension (9.1 ± 0.1 log CFU/mL) with a static contact angle of θ = 150.6° ± 1.0° (Figure S3), which is quite useful for various purposes such as stain release, lubricity, and water repelling.[36,37] Advancing and receding contact angle measurements revealed that water and bacteria suspension had contact angle hysteresis of ∼2.5° and ∼2.1°, respectively. Such low hysteresis indicates that RLLS surface is uniform and fairly homogeneous and that interaction between surface and liquid (or suspension) is weak.[38]

Slight differences in surface tensions of water (σ = 72.1 mN/m) and bacterial suspensions (σ = 66.3−69.7 mN/m) are likely to be responsible for ∼5.0° difference in static contact angle and dynamic contact angle measurements.[39] Approximately 85.0° increase in the contact angle changing from pristine quartz to methylated quartz is attributed to the surface chemistry effect, due to intrinsically low surface energy of the methyl group.[40] On the other hand, a difference of ∼60.0° in the contact angle of methylated quartz and RLLS is ascribed to the surface roughness and topography.[41]

3.4. Investigation of Bacterial Adhesion on RLLS under Static Conditions. Hydrodynamics can significantly influence the transport of bacteria from bulk liquid to surfaces.[42,43] Hence, bacterial adhesion to the developed surface was investigated under both static and dynamic conditions. Upon inoculating surfaces with bacterial suspension—i.e., *E. coli* O157:H7 or *S. aureus* at a concentration of 8.7−9.1 log CFU/mL under static conditions for 4 h—pristine quartz, hydrophobic quartz, and RLLS surfaces displayed significantly different bacterial adhesion behavior (Figure 3a−c). To be specific, for *E. coli* O157:H7, the pristine quartz surface supported the greatest bacterial adhesion with a mean density of 5.8 ± 0.0 log cells/mm^2. When the quartz was methylated, the bacterial adhesion significantly decreased to a mean density of 4.9 ± 0.1 log cells/mm^2. Ultimately, significantly less bacterial adhesion was detected on RLLS surfaces, counts were 2.7 ± 0.2 log cells/mm^2, corresponding to >99.9% reduction in bacterial adhesion in comparison to pristine quartz surfaces. As shown in Figure 3d−f, similar trends were also observed for *S. aureus*: the number of adherent bacteria decreased from 6.1 ± 0.0 to 2.9 ± 0.2 log cells/mm^2 upon changing the surface from pristine quartz to RLLS. A closer look at Figure 3c, f revealed that the attachment of bacteria was correlated with the existence of unpatterned regions (see Figure 2c) on RLLS. This result further highlights the importance of hollow nanodisc texture in preventing bacterial attachment (see Figure S4 for further comparison). Figure 3g summarizes these attachment behaviors of *E. coli* O157:H7 and *S. aureus* with respect to surface type.

3.5. Investigation of Bacterial Adhesion on RLLS under Dynamic Conditions. Prior studies have shown that the presence of a flow-field can facilitate or hinder the bacterial adhesion on a surface depending on the shear rates. In general, low shear rates result in an increased adhesion whereas high shear rates lead to a decreased adhesion.[44−46] Therefore, there is a need to ensure that the developed surfaces are also effective in reducing bacterial attachment under the flow conditions that promote bacterial adhesion. To this end, real-time bacterial adhesion behavior on RLLS was monitored using a customized flow chamber that imitates a typical fluidic channel of biosensor at low flow (shear) rates. The developed surface demonstrated excellent bacterial (Gram-negative *E. coli* O157:H7) antiadhesion properties during dynamic flow conditions (Figure 4a, b, and Movie S1, Movie S2, and Movie S3). Similar reduction trends were also observed against Gram-positive *S. aureus* (Movie S4). The number of adhering bacteria on RLLS was mostly constant during the continuous operation of 60 min, indicating the bacterial antiadhesion characteristics of these surfaces. On the other hand, the number of adhering bacteria increased linearly with increasing flow time for pristine and methylated quartz window surfaces (Figure 4c, d and Table S1). The previous studies reported that the initial stages of bacterial adhesion tend to follow a linear adhesion kinetics with respect to time,[47−50] which is consistent with the trends

DOI: 10.1021/acsami.5b05198
ACS Appl. Mater. Interfaces 2015, 7, 19274−19281

observed in pristine and methylated quartz surfaces. The loss of sensitivity in biosensors due to the accumulation of bacteria on flow chamber windows is a major problem in diagnostic assays.[51] The superior bacterial antiadhesion properties of RLLS window can help maintain sensor sensitivity by minimizing distortions in the light or laser path (i.e., interference, absorption, and reflection), flow direction, and flow velocity occurring through bacterial adhesion.

RLLS was chemically functionalized with a monolayer of TMCS in this study. If TMCS leaches away from the surfaces, it may lead to bacterial killing through an (unexpected) antibiotic effect. Hence, to determine whether the observed trends are indeed due to antiadhesion properties rather than an antimicrobial effect, a bacterial proliferation assay was performed. The data showed that the growth of bacterial cultures did not change in the presence of RLLS: bacterial concentrations reached ~8−9 log CFU/mL for both standard culture media (negative control) and standard culture media containing RLLS surface (Figure S5).

3.6. Possible Mechanisms of Bacterial Antiadhesion. The desirable antiadhesion characteristics can be attributed to two factors: (i) a large volume of air pockets (gaps) and (ii) a small ratio of the total rim area to the total projection area. First, the contact angle data indicated the superhydrophobic nature of RLLS. Superhydrophobic surfaces are associated with the transition from the Wenzel state to the Cassie−Baxter state and the formation of air pockets.[23] The presence of air pockets constitutes a physical barrier for bacteria to reach the material surfaces. Second, the structural characterization of hollow nanodiscs indicated that the areal ratio of solid/liquid interface to gas/liquid interface is small (i.e., ~0.06) due to their hollow nature. This information, coupled with the fact that the rim width (i.e., ~9 nm) of nanodiscs is much smaller than the length scales of bacteria (i.e., ~500−4000 nm), suggests a decreased probability for a bacterium to find a solid surface on which to attach itself (Figure S6).

3.7. Optical Transparency of RLLS. Although the developed materials have very promising bacterial antiadhesion and superhydrophobic properties, they cannot be used as the components of bio-optical devices unless these satisfy the optical-grade transparency, i.e., ≥92.0% within the visible light spectrum from 400 to 700 nm. It is a well-known challenge that typical surface topography and roughness modification strategies used for producing superhydrophobic surfaces lead to the loss of transparency to the levels below 90%, sometimes even down to 60%.[52] By inspiring from the outermost layers of rice leaves, we were able to produce surfaces with hollow nanodisc morphology, yielding optically transparent surfaces (Figure 5a, b). The comparison of transparency via UV−vis−NIR spectrophotometry indicated that pristine quartz (blue square) and RLLS (red circle) had a similar transmission level of 92% in the visible light spectrum. This is ascribed to the fact that root-mean-square (RMS) roughness of RLLS surfaces (~35 nm) and pristine quartz (~2 nm) was much smaller than the wavelength of visible light.[53]

3.8. Mechanical and Chemical Stability. For optically transparent materials, mechanical integrity and robustness of surface texture are important issues to consider because the optical transparency should not deteriorate under operational conditions. As such, RLLS was tested under standard sterilization condition, which is a 20 min sterilization process at 121 °C and 20 psi by autoclave. These conditions are much harsher than typical operation pressure (i.e., <15 psi) of biosensors and microfluidic devices.[54] It was found that, after autoclaving, no surface deformation occurred, surface superhydrophobicity remained the same, and bacterial antiadhesion properties and optical-grade transparency were also preserved, indicating robust durability of RLLS (Figure S7).

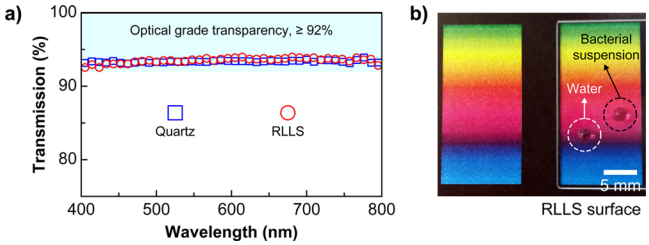

Figure 5. (a) Transmission spectra of pristine quartz (blue square) and RLLS (red circle) obtained by UV−vis−NIR spectrophotometry. (b) Wetting behavior of water and bacterial suspension on transparent RLLS surface.

In addition, devices and surfaces coming in contact with bacteria are generally sterilized with chemical sanitizers such as hydrogen peroxide (H_2O_2). Therefore, it is necessary to ensure the chemical stability of the developed bioinspired surfaces in such solutions. To this end, we investigated the chemical stability of functional groups of RLLS in 10% hydrogen peroxide solution over 3 weeks and observed no significant detachment of chemical groups and no change in wetting characteristics of the surface (Figure S8).

4. CONCLUSIONS

This study presents a single-step approach involving a templateless, self-masking reactive-ion etching for producing rice leaf-inspired surfaces that prevent microorganisms from attaching to them. In particular, bacterial repellency is demonstrated with respect to pathogenic Gram-negative *E. coli* O157:H7 and Gram-positive *S. aureus* under both static and dynamic conditions. The desirable bacterial antiadhesion characteristics of RLLS are ascribed to two factors associated with hollow nanodisc texture: (i) a large volume of air pockets (gaps) and (ii) a small areal ratio of solid/liquid interface to gas/liquid interface. One distinguishing feature of the developed rice leaf-inspired surfaces is that they also display optical-level transparency in the visible spectrum (i.e., ≥92% transmission). The combination of bacterial antiadhesion and optical transparency can be achieved presumably because of a reduced total roughness volume of hollow nanodiscs compared to solid (nonhollow) textures utilized in typical bacterial antiadhesion surfaces. Overall, a synergistic combination of bacterial antiadhesion properties and optical-grade transparency can open up new avenues in the design of antibiofouling surfaces and be beneficial for a broad set of applications and devices including biosensors; endoscopes; and microfluidic, bio-optical, lab-on-a-chip, and touchscreen devices.

■ ASSOCIATED CONTENT

Supporting Information

The Supporting Information is available free of charge on the ACS Publications website at DOI: 10.1021/acsami.5b05198.

SEM micrographs, contact angle measurements, plate-counting results, photograph of autoclave sterilization, ATR-FTIR data, and XPS data (PDF)

DOI: 10.1021/acsami.5b05198
ACS Appl. Mater. Interfaces 2015, 7, 19274−19281

Movie from flow chamber experiments: RLLS (*E. coli* O157:H7, after 10 min, 20 min, 40 min, and 60 min) (PDF)

Movie from flow chamber experiments: uncoated quartz (*E. coli* O157:H7, after 60 min) (PDF)

Movie from flow chamber experiments: coated quartz (*E. coli* O157:H7, after 60 min) (PDF)

Movie from flow chamber experiments: RLLS (*S. aureus*, after 60 min) (PDF)

AUTHOR INFORMATION

Corresponding Author

*E-mail: makbulut@tamu.edu.

Author Contributions

The manuscript was written through contributions of all authors. All authors have given approval to the final version of the manuscript.

Funding

This project was partially supported by Agriculture and Food Research Initiative Competitive Grant no. 2011-67017-30028 from the USDA National Institute of Food and Agriculture to M.A. and L.C.-Z., by National Science Foundation (NSF) Grant no. 1434421 to M.A. and J.K.O., and by NSF Grant no. 1511626 to X.L. and Y.M. Acknowledgment is made to the Donors of the American Chemical Society Petroleum Research Fund for partial support of this research.

Notes

The authors declare no competing financial interest.

ACKNOWLEDGMENTS

We would like to thank Dr. Larry D. Godfrey, Department of Entomology and Nematology, University of California, Davis, CA, U.S.A. and Kevin Goding for providing rice leaf samples.

REFERENCES

(1) Hall-Stoodley, L.; Costerton, J. W.; Stoodley, P. Bacterial Biofilms: from the Natural Environment to Infectious Diseases. *Nat. Rev. Microbiol.* **2004**, *2*, 95−108.

(2) Campoccia, D.; Montanaro, L.; Arciola, C. R. A Review of the Biomaterials Technologies for Infection-Resistant Surfaces. *Biomaterials* **2013**, *34*, 8533−8554.

(3) Banerjee, I.; Pangule, R. C.; Kane, R. S. Antifouling Coatings: Recent Developments in the Design of Surfaces that Prevent Fouling by Proteins, Bacteria, and Marine Organisms. *Adv. Mater.* **2011**, *23*, 690−718.

(4) Puckett, S. D.; Taylor, E.; Raimondo, T.; Webster, T. J. The Relationship between the Nanostructure of Titanium Surfaces and Bacterial Attachment. *Biomaterials* **2010**, *31*, 706−713.

(5) Xu, L.-C.; Siedlecki, C. A. Submicron-Textured Biomaterial Surface Reduces *Staphylococcal* Bacterial Adhesion and Biofilm Formation. *Acta Biomater.* **2012**, *8*, 72−81.

(6) Epstein, A. K.; Wong, T.-S.; Belisle, R. A.; Boggs, E. M.; Aizenberg, J. Liquid-Infused Structured Surfaces with Exceptional Anti-Biofouling Performance. *Proc. Natl. Acad. Sci. U. S. A.* **2012**, *109*, 13182−13187.

(7) Shivapooja, P.; Wang, Q.; Orihuela, B.; Rittschof, D.; Lõpez, G. P.; Zhao, X. Bioinspired Surfaces with Dynamic Topography for Active Control of Biofouling. *Adv. Mater.* **2013**, *25*, 1430−1434.

(8) Rasko, D. A.; Sperandio, V. Anti-Virulence Strategies to Combat Bacteria-Mediated Disease. *Nat. Rev. Drug Discovery* **2010**, *9*, 117−128.

(9) Xu, L.; Karunakaran, R. G.; Guo, J.; Yang, S. Transparent, Superhydrophobic Surfaces from One-Step Spin Coating of Hydrophobic Nanoparticles. *ACS Appl. Mater. Interfaces* **2012**, *4*, 1118−1125.

(10) Deng, X.; Mammen, L.; Butt, H.-J.; Vollmer, D. Candle Soot as a Template for a Transparent Robust Superamphiphobic Coating. *Science* **2012**, *335*, 67−70.

(11) Rahmawan, Y.; Xu, L.; Yang, S. Self-Assembly of Nanostructures towards Transparent, Superhydrophobic Surfaces. *J. Mater. Chem. A* **2013**, *1*, 2955−2969.

(12) Massad-Ivanir, N.; Shtenberg, G.; Zeidman, T.; Segal, E. Construction and Characterization of Porous SiO_2/Hydrogel Hybrids as Optical Biosensors for Rapid Detection of Bacteria. *Adv. Funct. Mater.* **2010**, *20*, 2269−2277.

(13) McConney, M. E.; Anderson, K. D.; Brott, L. L.; Naik, R. R.; Tsukruk, V. V. Bioinspired Material Approaches to Sensing. *Adv. Funct. Mater.* **2009**, *19*, 2527−2544.

(14) Vogelmann, T. C. Plant Tissue Optics. *Annu. Rev. Plant Physiol. Plant Mol. Biol.* **1993**, *44*, 231−251.

(15) Mandoli, D. F.; Briggs, W. R. Optical Properties of Etiolated Plant Tissues. *Proc. Natl. Acad. Sci. U. S. A.* **1982**, *79*, 2902−2906.

(16) Fukshansky, L.; Fukshansky-Kazarinova, N.; Remisowsky, A. M. v. Estimation of Optical Parameters in a Living Tissue by Solving the Inverse Problem of the Multiflux Radiative Transfer. *Appl. Opt.* **1991**, *30*, 3145−3153.

(17) Vogelmann, T. C.; Bornman, J. F.; Yates, D. J. Focusing of Light by Leaf Epidermal Cells. *Physiol. Plant.* **1996**, *98*, 43−56.

(18) Smyth, C. J.; Jonsson, P.; Olsson, E.; Söderlind, O.; Rosengren, J.; Hjertén, S.; Wadström, T. Differences in Hydrophobic Surface Characteristics of Porcine Enteropathogenic *Escherichia coli* with or without K88 Antigen as Revealed by Hydrophobic Interaction Chromatography. *Infect. Immun.* **1978**, *22*, 462−472.

(19) Kwok, D. Y.; Neumann, A. W. Contact Angle Measurement and Contact Angle Interpretation. *Adv. Colloid Interface Sci.* **1999**, *81*, 167−249.

(20) Koch, K.; Bhushan, B.; Barthlott, W. Diversity of Structure, Morphology and Wetting of Plant Surfaces. *Soft Matter* **2008**, *4*, 1943−1963.

(21) Wu, D.; Wang, J. N.; Wu, S. Z.; Chen, Q. D.; Zhao, S.; Zhang, H.; Sun, H. B.; Jiang, L. Three-Level Biomimetic Rice-Leaf Surfaces with Controllable Anisotropic Sliding. *Adv. Funct. Mater.* **2011**, *21*, 2927−2932.

(22) Truong, V. K.; Lapovok, R.; Estrin, Y. S.; Rundell, S.; Wang, J. Y.; Fluke, C. J.; Crawford, R. J.; Ivanova, E. P. The Influence of Nano-Scale Surface Roughness on Bacterial Adhesion to Ultrafine-Grained Titanium. *Biomaterials* **2010**, *31*, 3674−3683.

(23) Chen, L.; Yang, G.; Wang, S. Air-Grid Surface Patterning Provided by Superhydrophobic Surfaces. *Small* **2012**, *8*, 962−965.

(24) Min, W. L.; Jiang, B.; Jiang, P. Bioinspired Self-Cleaning Antireflection Coatings. *Adv. Mater.* **2008**, *20*, 3914−3918.

(25) Lu, W.; Lieber, C. M. Nanoelectronics from the Bottom Up. *Nat. Mater.* **2007**, *6*, 841−850.

(26) Feng, L.; Zhang, Y.; Xi, J.; Zhu, Y.; Wang, N.; Xia, F.; Jiang, L. Petal Effect: A Superhydrophobic State with High Adhesive Force. *Langmuir* **2008**, *24*, 4114−4119.

(27) Hensel, R.; Finn, A.; Helbig, R.; Braun, H. G.; Neinhuis, C.; Fischer, W. J.; Werner, C. Biologically Inspired Omniphobic Surfaces by Reverse Imprint Lithography. *Adv. Mater.* **2014**, *26*, 2029−2033.

(28) Pokroy, B.; Epstein, A. K.; Persson-Gulda, M. C. M.; Aizenberg, J. Fabrication of Bioinspired Actuated Nanostructures with Arbitrary Geometry and Stiffness. *Adv. Mater.* **2009**, *21*, 463−469.

(29) Jansen, H.; Gardeniers, H.; de Boer, M.; Elwenspoek, M.; Fluitman, J. A Survey on the Reactive Ion Etching of Silicon in Microtechnology. *J. Micromech. Microeng.* **1996**, *6*, 14−28.

(30) Hedlund, C.; Lindberg, U.; Bucht, U.; Soderkvist, J. Anisotropic Etching of Z-Cut Quartz. *J. Micromech. Microeng.* **1993**, *3*, 65−73.

(31) Stoffels, W. W. Polymerization of Fluorocarbons in Reactive Ion Etching Plasmas. *J. Vac. Sci. Technol., A* **1998**, *16*, 87−95.

(32) Lohmüller, T.; Helgert, M.; Sundermann, M.; Brunner, R.; Spatz, J. P. Biomimetic Interfaces for High-Performance Optics in the Deep-UV Light Range. *Nano Lett.* **2008**, *8*, 1429−1433.

(33) Hsu, C.-H.; Lo, H.-C.; Chen, C.-F.; Wu, C. T.; Hwang, J.-S.; Das, D.; Tsai, J.; Chen, L.-C.; Chen, K.-H. Generally Applicable Self-

DOI: 10.1021/acsami.5b05198
ACS Appl. Mater. Interfaces 2015, 7, 19274−19281

Masked Dry Etching Technique for Nanotip Array Fabrication. *Nano Lett.* **2004**, *4*, 471−475.
(34) Chandler, D. Interfaces and the Driving Force of Hydrophobic Assembly. *Nature* **2005**, *437*, 640−647.
(35) Zhang, X.; Shi, F.; Niu, J.; Jiang, Y.; Wang, Z. Superhydrophobic Surfaces: from Structural Control to Functional Application. *J. Mater. Chem.* **2008**, *18*, 621−633.
(36) Blossey, R. Self-Cleaning Surfaces — Virtual Realities. *Nat. Mater.* **2003**, *2*, 301−306.
(37) Quirynen, M.; Bollen, C. M. L. The Influence of Surface-Roughness and Surface-Free Energy on Supragingival and Subgingival Plaque-Formation in Man. *J. Clin. Periodontol.* **1995**, *22*, 1−14.
(38) Gao, L.; McCarthy, T. J. Contact Angle Hysteresis Explained. *Langmuir* **2006**, *22*, 6234−6237.
(39) Absolom, D. R.; Lamberti, F. V.; Policova, Z.; Zingg, W.; van Oss, C. J.; Neumann, A. W. Surface Thermodynamics of Bacterial Adhesion. *Appl. Environ. Microbiol.* **1983**, *46*, 90−97.
(40) Ma, M.; Hill, R. M. Superhydrophobic Surfaces. *Curr. Opin. Colloid Interface Sci.* **2006**, *11*, 193−202.
(41) Wenzel, R. N. Surface Roughness and Contact Angle. *J. Phys. Colloid Chem.* **1949**, *53*, 1466−1467.
(42) Rijnaarts, H. H. M.; Norde, W.; Bouwer, E. J.; Lyklema, J.; Zehnder, A. J. B. Bacterial Adhesion under Static and Dynamic Conditions. *Appl. Environ. Microbiol.* **1993**, *59*, 3255−3265.
(43) Lecuyer, S.; Rusconi, R.; Shen, Y.; Forsyth, A.; Vlamakis, H.; Kolter, R.; Stone, H. A. Shear Stress Increases the Residence Time of Adhesion of *Pseudomonas aeruginosa*. *Biophys. J.* **2011**, *100*, 341−350.
(44) Thomas, W. E.; Trintchina, E.; Forero, M.; Vogel, V.; Sokurenko, E. V. Bacterial Adhesion to Target Cells Enhanced by Shear Force. *Cell* **2002**, *109*, 913−923.
(45) Mannoor, M. S.; Zhang, S.; Link, A. J.; McAlpine, M. C. Electrical Detection of Pathogenic Bacteria via Immobilized Antimicrobial Peptides. *Proc. Natl. Acad. Sci. U. S. A.* **2010**, *107*, 19207−19212.
(46) Emerson, R. J.; Camesano, T. A. Nanoscale Investigation of Pathogenic Microbial Adhesion to a Biomaterial. *Appl. Environ. Microbiol.* **2004**, *70*, 6012−6022.
(47) Busscher, H. J.; Uyen, M. H.; van Pelt, A. W.; Weerkamp, A. H.; Arends, J. Kinetics of Adhesion of the Oral Bacterium *Streptococcus sanguis* CH3 to Polymers with Different Surface Free Energies. *Appl. Environ. Microbiol.* **1986**, *51*, 910−914.
(48) Pranzetti, A.; Salaün, S.; Mieszkin, S.; Callow, M. E.; Callow, J. A.; Preece, J. A.; Mendes, P. M. Model Organic Surfaces to Probe Marine Bacterial Adhesion Kinetics by Surface Plasmon Resonance. *Adv. Funct. Mater.* **2012**, *22*, 3672−3681.
(49) Lüdecke, C.; Jandt, K. D.; Siegismund, D.; Kujau, M. J.; Zang, E.; Rettenmayr, M.; Bossert, J.; Roth, M. Reproducible Biofilm Cultivation of Chemostat-Grown *Escherichia coli* and Investigation of Bacterial Adhesion on Biomaterials Using a Non-Constant-Depth Film Fermenter. *PLoS One* **2014**, *9*, e84837.
(50) Mohamed, N.; Rainier, T. R.; Ross, J. M. Novel Experimental Study of Receptor-Mediated Bacterial Adhesion under the Influence of Fluid Shear. *Biotechnol. Bioeng.* **2000**, *68*, 628−636.
(51) Bhatia, S. N.; Ingber, D. E. Microfluidic Organs-On-Chips. *Nat. Biotechnol.* **2014**, *32*, 760−772.
(52) Wong, T.-S.; Kang, S. H.; Tang, S. K. Y.; Smythe, E. J.; Hatton, B. D.; Grinthal, A.; Aizenberg, J. Bioinspired Self-Repairing Slippery Surfaces with Pressure-Stable Omniphobicity. *Nature* **2011**, *477*, 443−447.
(53) Nakajima, A.; Fujishima, A.; Hashimoto, K.; Watanabe, T. Preparation of Transparent Superhydrophobic Boehmite and Silica Films by Sublimation of Aluminum Acetylacetonate. *Adv. Mater.* **1999**, *11*, 1365−1368.
(54) Laser, D. J.; Santiago, J. G. A Review of Micropumps. *J. Micromech. Microeng.* **2004**, *14*, R35−R64.

DOI: 10.1021/acsami.5b05198
ACS Appl. Mater. Interfaces 2015, 7, 19274−19281